DOI: 10.18462/iir.tptpr2025.1124

Consideration and evaluation of the velocity slip for improved prediction of the refrigerant charge

Tim RUDZIK*, Max KUNATH, Yixia XU, Christiane THOMAS
Technische Universität Dresden
Schaufler Chair of Refrigeration, Cryogenics and Compressor Technology
Dresden, Saxony, 01069, Germany
*Corresponding author: tim.rudzik@tu-dresden.de

ABSTRACT

Process simulations are becoming central to heat pump design. In particular, the simulative analysis of the refrigerant charge is proving to be increasingly important, especially with R-290 (propane) gaining traction in European installations.
An important influence on the amount of refrigerant in the system components is the velocity slip between gas and liquid. Different phase velocities cause liquid refrigerant accumulation. Taking the velocity slip into account leads to an increase in the calculated charge quantity required for optimum system operation.
This paper presents the velocity slip implementation in a heat pump model using the Modelica TIL-library, to investigate its influence on the system behavior. Different slip models are compared with each other, also focusing on the impact of different refrigerants and their properties.
The results indicate that the consideration of slip in the process simulation has a significant influence on the system behavior and the refrigerant requirement for optimum operation.

Keywords: Heat pumps, Slip ratio, Void fraction, Refrigerant charge, System simulation, Hydrocarbons, R-290

1 INTRODUCTION

Refrigeration systems and heat pumps play a vital role in various applications, and trends now favor hydrocarbon refrigerants like R-290 because of their lower environmental impact. However, their flammability requires reduced refrigerant charges for safe operation, making accurate simulation models essential for optimizing component design.
Conventional simulation models (e.g., the TIL-Suite from TLK Energy, 2024) typically assume equal gas and liquid velocities (a slip ratio of one), thereby neglecting the real differences that affect refrigerant distribution in evaporators and condensers—and ultimately, system efficiency and charge.
The literature presents several slip correlations to address this phenomenon. Wedekind et al. (1978) introduced a simple method using an average void fraction, later adopted by Shah et al. (2004) and Rasmussen (2012). Assawamartbunlue et al. (2000) demonstrated that both the choice of the slip correlation and the condenser inlet air temperature significantly affect the charge in the liquid receiver, while Abdelaziz et al. (2008) confirmed the suitability of these correlations for dynamic simulations.
To date, however, no publications known to the authors have addressed the consideration of different slip correlations in process simulations with volume-discretized pipes and heat exchangers. This work aims to close this research gap by implementing multiple slip correlations in a Modelica-based simulation to assess the steady-state refrigerant charge and system performance of a residential heat pump using R-290 (propane) as the refrigerant. Also, the amount of refrigerant in the condenser is evaluated for various refrigerants and slip correlations. The findings aim to improve simulation accuracy and to support the development of safer, more efficient systems.

2 FUNDAMENTAL DEFINITIONS AND DESCRIPTION OF THE MODELS

2.1 Slip Ratio

In the context of this work, the slip ratio is defined as the ratio of the velocities between the gaseous and liquid phases of a substance, given for refrigerants by (VDI 2013, S. 1287):

$$S = \frac{w_g}{w_l} = \frac{\dot{x}}{(1-\dot{x})} \cdot \frac{(1-vF)}{vF} \cdot \frac{\rho_l}{\rho_g} \quad \text{Eq. (1)}$$

Here, w_g and w_l denote the velocities of the gas and the liquid phases, respectively; $\dot{x}$ represents the vapor mass fraction in the flow, ρ_l and ρ_g denote the densities of the liquid and gas phases. Additionally, vF (*void fraction*) is defined as the volume fraction of the gas V_g relative to the total considered volume V_{tot}:

$$vF = \frac{V_g}{V_{tot}} \quad \text{Eq. (2)}$$

By definition, both S and vF can only appear in components where two-phase flow is present, which in the case of heat pumps occurs mainly in the evaporator and condenser.
Numerous experiments using various fluids and conditions have quantified the slip ratio (or void fraction), leading to correlations (e.g., Graham et al. 1997; Wilson et al. 1998) and subsequent comparative evaluations (Rice 1987). Abdelaziz et al. (2008) offer a comprehensive overview of the various correlations for S and vF, organizing them into distinct groups - a classification that is briefly introduced in the following paragraphs:

Slip correlations compute vF with Eq. (3), where different dependencies for S arise, depending on the chosen correlation. If it is assumed that there is no velocity difference between the phases (S = 1), this corresponds to the homogeneous correlation vF_h.

$$vF = \left(1 + \frac{1-\dot{x}}{\dot{x}} \cdot \frac{\rho_g}{\rho_l} \cdot S\right)^{-1} \quad \text{Eq. (3)}$$

K- vF - correlations are based on the homogeneous correlation vF_h multiplied by a factor K which can be either constant or prescribed as a function of various parameters, such as $\dot{x}$:

$$vF = K \cdot vF_h \quad \text{Eq. (4)}$$

Slip correlations based on the drift-flux method always have the form:

$$vF = \frac{w_{sg}}{C_o \cdot w_m + w_{gm}} \quad \text{Eq. (5)}$$

Here, w_{sg} is the superficial gas velocity, calculated as the gas volumetric flow rate divided by the total cross-sectional area, w_m is the mean velocity of the two-phase flow, defined as total volumetric flow rate divided by the total cross-sectional area, C_0 is the distribution parameter, and w_{gm} is the drift velocity, defined as the difference between the actual gas velocity and w_m. In the case of the homogeneous correlation, w_{gm} is equal to zero and $C_0 = 1$.
Some correlations additionally depend on mass flux and dimensionless parameters such as the Froude and Reynolds numbers, while others are classified using the Lockhart-Martinelli parameter X_{tt}.
Xu et al. (2014) used a similar categorization to analyze various slip correlations based on experimental data from different refrigerants and geometries, and they developed a new correlation in the process. Their analysis showed that the correlations by Chisholm (1973), Yashar et al., Smith (1969), Massena, Huq-Loth, Steiner, Premoli et al., and Osmachkin-Borisov exhibited the smallest deviations from experimental data,

even though they were not originally developed for refrigerants.
Based on the literature review, eight slip (or void fraction) correlations were selected for the investigations presented in this paper. Since Xu et al. (2014) provided an in-depth analysis of the deviations of the individual correlations from the measured data points, the correlation following their method is used in the subsequent considerations.
The chosen correlations for the slip ratio S and void fraction vF can be found in Table 1.

Table 1: Selection of correlations for slip ratio and void fraction

Correlation	S	vF	Comment
Homogeneous		$vF_h = \left(1 + \frac{1-\dot{x}}{\dot{x}} \frac{\rho_g}{\rho_l}\right)^{-1}$	
Xu et al. (2014)		$vF = \left(1 + (1 + 2 \cdot Fr_l^{-0.2} vF_h^{3.5}) \cdot \left(\frac{1-\dot{x}}{\dot{x}}\right) \cdot \left(\frac{\rho_g}{\rho_l}\right)\right)^{-1}$	horiz. and vertical pipes; R-134a, R-410A, R-11, R-12, R-22
Chisholm (1973)	$S = \left(1 - \dot{x} + \dot{x} \cdot \frac{\rho_l}{\rho_g}\right)^{\frac{1}{2}}$		pipes; water
Lockhart and Martinelli (L.-M.) (Xu et al. 2014)		$vF = (1 + 0.28 \cdot X_{tt}^{0.71})^{-1}$ $X_{tt} = \left(\frac{1-\dot{x}}{\dot{x}}\right)^{0.9} \cdot \left(\frac{\rho_g}{\rho_l}\right)^{0.5} \cdot \left(\frac{\eta_l}{\eta_g}\right)^{0.1}$	pipes; air-water
Osmachkin and Borisov (O.-B.) (Xu et al. 2014)	$S = 1 + \frac{0.6 + 1.5 \cdot vF_h^2}{Fr_l^{0.25}} \left(1 - \frac{p}{p_{cr}}\right)$ $Fr_l = \frac{G^2}{g \cdot D \cdot \rho_l^2}$		vertical pipes; water
Smith (1969)		$vF = \left(1 + \frac{1-\dot{x}}{\dot{x}} \cdot \frac{\rho_g}{\rho_l} \cdot (K + (1-K)) \sqrt{\frac{\frac{\rho_l}{\rho_g} + \frac{K \cdot (1-\dot{x})}{\dot{x}}}{1 + \frac{K \cdot (1-\dot{x})}{\dot{x}}}}\right)^{-1}$	horiz. and vertical pipes; water, air-water; K = 0.4
Massena (Xu et al. 2014)		$vF = \begin{cases} 0.833 \cdot vF_h & for\ vF_h < 0.9 \\ (0.833 + (1 - 0.833) \cdot \dot{x}) \cdot vF_h & for\ vF_h \geq 0.9 \end{cases}$	pipes; water
Steiner (VDI 2013, S. 1289)		$C_0 = 1 + 0.12 \cdot (1 - \dot{x})$ $U_{gm} = \frac{1.18 \cdot (1-\dot{x})}{\rho_l^{0.5}} \cdot \left(g \cdot \sigma \cdot (\rho_l - \rho_g)\right)^{0.25}$ $vF = \frac{w_{sg}}{C_o \cdot w_m + w_{gm}}$	rectangular channels and pipes; water
Rigot (Abdelaziz 2008)	$S = 2$		

2.2 **Model Implementation**

2.2.1 Influence of the Slip Ratio on the Modeling of One-Dimensional Fluid Volumes

Before explaining the implementation of varying slip ratios in an existing process simulation, its influence is first illustrated using Figure 1. This figure shows two one-dimensional, adiabatic volume cells: on the left, with a slip ratio of one, and on the right with $S > 1$. In both diagrams, the phase velocities w_g and w_l are shown, as well as the cross-sectional areas A_g and A_l for the gas and liquid phases respectively.

A distinction is made between the boundaries of the local cell (blue square) and those of the circulating mass flow (colored and dashed). In the left-hand illustration of Figure 1, the velocities of the gas and liquid phases are equal ($w_g = w_l$), so that the entire fluid in both phases leaves the local cell synchronously. Consequently, the vapor mass fraction $\dot{x}$ of the exiting mass flow is identical to the local vapor mass fraction x. In contrast, in Figure 1 on the right, the gas velocity w_g is higher than the liquid velocity w_l. In this case, during the time interval $\triangle$t in which the entire gas volume of the local cell passes the left boundary, only a portion of the liquid volume does so. As a result, the boundaries of the mass flow and of the local cell differ, and $\dot{x}$ becomes larger than the local value x.

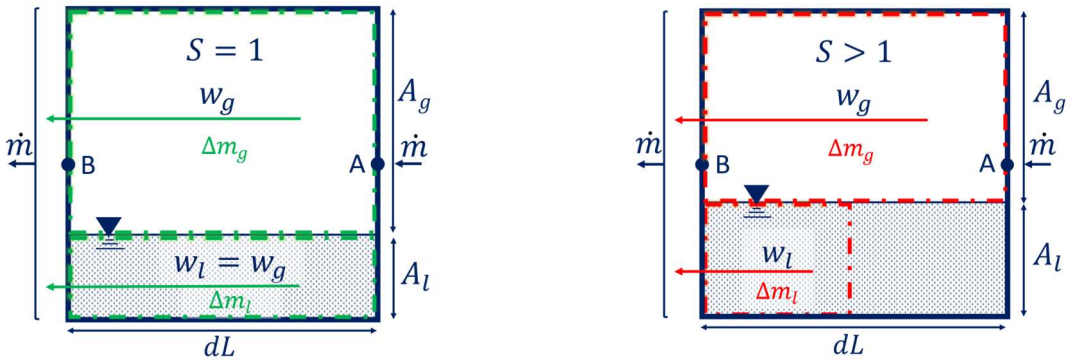

Figure 1: Schematic illustration of an adiabatic volume cell with $S = 1$ (left) and $S > 1$ (right) under steady-state conditions.

Furthermore, a slip ratio of $S > 1$ results in a higher liquid level and, thereby, a greater cell mass compared to the case with equal phase velocities. This effect follows from the continuity equation for the steady mass flow $\dot{m}$:

$$A_g \cdot w_g \cdot \rho_g + A_l \cdot w_l \cdot \rho_l = \dot{m} \qquad \text{Eq. (6)}$$

Using Eq. (1) and Eq. (6), the ratio of the cross-sectional areas for gas A_g and liquid A_l as a function of the slip ratio S and the vapor mass fraction $\dot{x}$ can be expressed as:

$$\frac{A_g}{A_l} = \frac{\dot{x}}{S \cdot (1 - \dot{x})} \cdot \frac{\rho_l}{\rho_g} \qquad \text{Eq. (7)}$$

Eq. (7) shows that the area ratio A_g / A_l decreases with increasing S, which in turn leads to an increase in the liquid level and thus the cell mass.

2.2.2 Standard Model without Velocity Slip

To investigate the effects of the velocity slip on important cycle criteria such as refrigerant charge and system efficiency by simulation, the approach described above and the necessary equations were first implemented in an existing system. The basis for this was the TIL-Suite from TLK Energy, in which heat exchangers are discretized into multiple volume cells.

Within each volume cell, having the ports A and B (see Figure 1, left), the three conservation equations for mass, momentum, and energy are solved in one dimension, and the calculated quantities are passed on to the next cell along the flow. In describing mass conservation, the transient case also accounts for the time variation of the density of the volume element $d\rho$ / dt:

$$\frac{d\rho}{dt} \cdot V = \dot{m}_A + \dot{m}_B \quad \text{Eq. (8)}$$

The momentum balance is limited to the frictional pressure drop $\triangle p$ of the flow, which can be prescribed by a correlation. Acceleration pressure losses and gravitational effects are not considered:

$$p_A - p_B = \triangle p \quad \text{Eq. (9)}$$

From the energy balance, the specific enthalpy h of the cell is determined by taking into account the enthalpy fluxes in and out, the heat input $\dot{Q}$, and the technical work:

$$\frac{dh}{dt} \cdot m = \dot{m}_A \cdot (h_A - h) + \dot{m}_B \cdot (h_B - h) + \dot{Q} + V \cdot \frac{dp}{dt} \quad \text{Eq. (10)}$$

For the calculation of $\dot{Q}$, a heat transfer correlation must be provided. h_A and h_B represent the specific enthalpies of the incoming and outgoing mass flows, respectively. In addition, the mass m of the cell is calculated by:

$$m = V \cdot \rho \quad \text{Eq. (11)}$$

The cell density ρ is determined from the pressure p and the specific enthalpy h using fluid property calculations of the TIL-Suite (TILMedia).

Under the simplified assumption of identical velocities for gas and liquid (S = 1, see Figure 1, left) in the two-phase region and for a flow from A to B it further follows that:

$$h_B = h \quad \text{Eq. (12)}$$

In this case, the specific enthalpy h in the local cell is also the enthalpy h_B of the exiting mass flow.

To incorporate the slip phenomenon into the framework described above, two approaches were developed, and are explained below.

2.2.3 Slip-Ratio-Based Enthalpy Determination (Base Model)

In the approach of the slip-ratio-based enthalpy determination, it proved expedient to decouple the circulating and local fluid properties, which differ solely due to the velocity slip. In this approach, the original conservation equations remain unchanged in form, but now they specifically calculate the thermodynamic properties of the two phases within the cell rather than the properties of the outgoing mass flow. This is achieved by extending Eq. (12) as follows (for the flow from A to B):

$$h_B = \dot{x} \cdot h_g + (1 - \dot{x}) \cdot h_l \quad \text{Eq. (13)}$$

Thus, the specific enthalpy h_B passed to the next cell corresponds to that of the circulating fluid, which is determined with the help of the specific enthalpies h_g of the gas and h_l of the liquid as well as the vapor mass fraction $\dot{x}$ of the circulating fluid.

For the calculation of $\dot{x}$, Eq. (1) is implemented, which describes the relationship between local and circulating quantities via the slip ratio S and the void fraction vF. Additionally, vF is defined from the local properties of the cell:

$$vF = \frac{x \cdot \rho}{\rho_g} \quad \text{Eq. (14)}$$

Note the introduction of the vapor mass fraction in the (stationary) cell x.

To complete the system of equations, either S or vF needs to be specified. This can be done via a correlation,

a physical model, or a constant value.
Since the fluid properties in the volume cells are determined from the enthalpy and pressure ($f(h,p)$), the implementation of the velocity slip only affects the local values of the volume cells. However, for pressure drop and heat transfer correlations, the circulating properties are relevant. Therefore, an additional calculation of these fluid properties ($f(h_B,p)$) is required, which entails increased computational effort in the basic model.

2.2.4 Slip-Ratio-Based Mass Determination (Simplified Model)

To assess the effect of the slip ratio on the fluid mass in each cell, it is not necessary to enforce a strict separation between local and circulating properties. Alternatively, the cell mass can be computed in a slip-specific manner. In this case, the density ρ in Eq. (11) is defined via vF and the assumption of steady continuity:

$$m = V \cdot (vF \cdot (\rho_g - \rho_l) + \rho_l) \qquad \text{Eq. (15)}$$

The void fraction vF is either prescribed by a correlation or calculated using Eq. (3) in conjunction with a slip correlation. The cell mass is then obtained in this case by specifying S (Eq. (3) in Eq. (15)):

$$m = V \cdot \rho_g \cdot \frac{1 + \frac{1-\dot{x}}{\dot{x}} \cdot S}{1 + \frac{1-\dot{x}}{\dot{x}} \frac{\rho_g}{\rho_l} \cdot S} \qquad \text{Eq. (16)}$$

The simplified model differs from the base model in two key ways: it calculates the cell mass using the assumption of steady state continuity, and it does not require separate treatment of local and circulating fluid properties. A systematic comparison revealed that, while transient responses vary slightly between the two models, both yield nearly identical steady-state results. Since the current investigation focuses solely on steady-state behavior, the simplified model was chosen due to its computational efficiency and improved numerical stability. (For control-oriented studies that demand a detailed transient response, the basic model might be more appropriate.)

2.3 System Definition and Simulation Boundary Conditions

The subject of these investigations is the model of a fictitious air-to-air heat pump (four-component cycle without a receiver, using the refrigerant R-290, operating at 7 °C/20 °C, with 10 K superheat) with a maximum heating capacity of 10 kW. Realistic component sizes are considered in the design process. The key boundary conditions are shown in Figure 2.

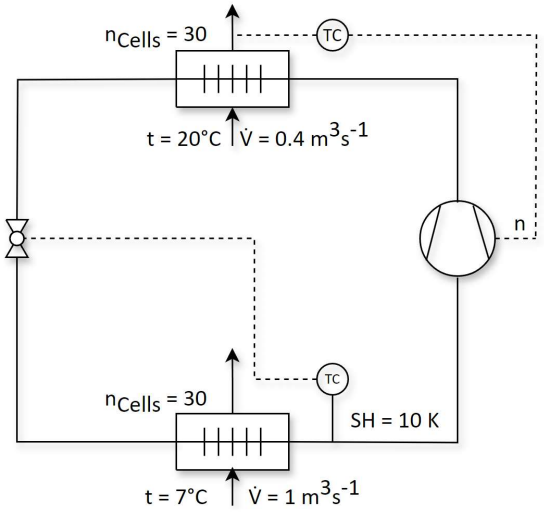

Figure 2: Schematic illustration of the simulated heat pump model

The mass flow rate and the indicated compressor power P_i of the compressor were implemented using a 10-coefficient polynomial according to Eq. (17).

$$\dot{m} \dots P_i = \frac{n}{n_{ref}} \cdot f(a_1 \dots a_{10}, t_0, t_c) \qquad \text{Eq. (17)}$$

The dependency on the rotational speed of the compressor n was taken into account as a factor relative to the nominal rotational speed n_{ref} given in the data sheet; however, the dependence of the isentropic and volumetric efficiency on rotational speed was not considered. The influence of the superheat was incorporated via a correlation according to Shen et al. (2009).

The geometric parameters and the heat transfer correlations for both fin and tube heat exchangers (condenser and evaporator) are identical and are listed in Table 2. Pressure drops were not considered either in the heat exchangers or in the piping.

Table 2: Parameters of the fin and tube heat exchangers (condenser and evaporator)

Parameter	Value
Inner tube diameter	6 mm
Outer tube diameter	8 mm
Length	745 mm
Number of tubes: horizontal/vertical	2 / 32
Tube spacing: horizontal/vertical	26 mm / 15 mm
Fins: thickness/spacing	0.1 mm / 0.215 mm
Heat transfer: evaporation	Steiner (VDI 2013, S. 915)
Heat transfer: condensation	Shah (1979)
Single-phase heat transfer	Gnielinski-Dittus-Boelter (Baer et al. 1996)
Air-side heat transfer	Haaf (Steimle et al. 1988, S. 435 ff.)
Number of cells for discretization	30

3 SIMULATION STUDIES AND RESULTS

3.1 Analysis at Constant Subcooling

Maintaining 8 K subcooling, the heating capacity was varied from 4 kW to 10 kW by adjusting the rotational speed of the compressor to study the effect of different slip correlations on the required refrigerant charge. As shown in Figure 3, incorporating slip ratios of $S > 1$ increases the required charge relative to the homogeneous case ($S = 1$, Ref). The increase depends primarily on the chosen slip model - e.g., the Osmachkin-Borisov correlation shows a modest increase of about 5.7 % at 10 kW, whereas the Massena correlation can lead to increases of up to 24.8 % at 6 kW. Although variations in heating capacity influence system pressures and heat transfer, their effect on the charge is secondary to the slip correlation used.

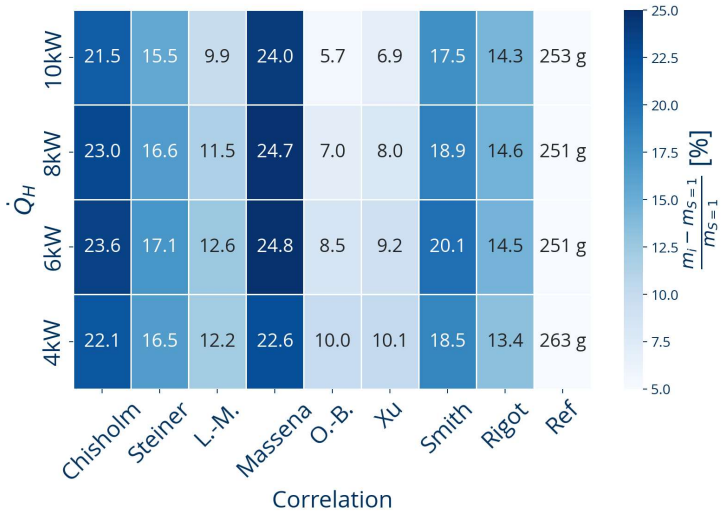

Figure 3: Relative change in system charge compared to $S = 1$ (Ref) for different correlations and heating capacities (Ref shows total mass)

Figure 4 presents the slip ratio as a function of the vapor quality in both the condenser and the evaporator. Generally, the slip ratio rises with increasing vapor quality; however, notable differences emerge between the models. The Lockhart-Martinelli correlation, for example, predicts slip ratios below one near the condenser outlet and then a strong increase at high vapor qualities, while the Massena correlation exhibits a discontinuity due to a case differentiation at vF_h = 0.9 (see Table 1). In contrast, the Osmachkin-Borisov and Xu correlations display a relatively flat increase of the slip ratio along the heat exchanger length.

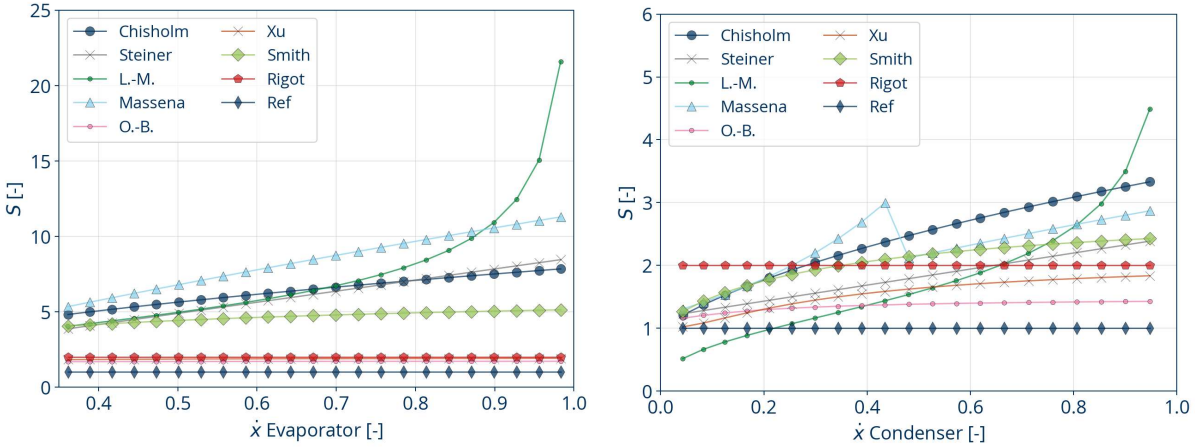

Figure 4: Slip ratio S as a function of vapor quality $\dot{x}$ in the evaporator (left) and condenser (right) at $\dot{Q}_H = 10$ kW

The impact of these differences in S is also evident in the mass distribution per cell (Figure 5).

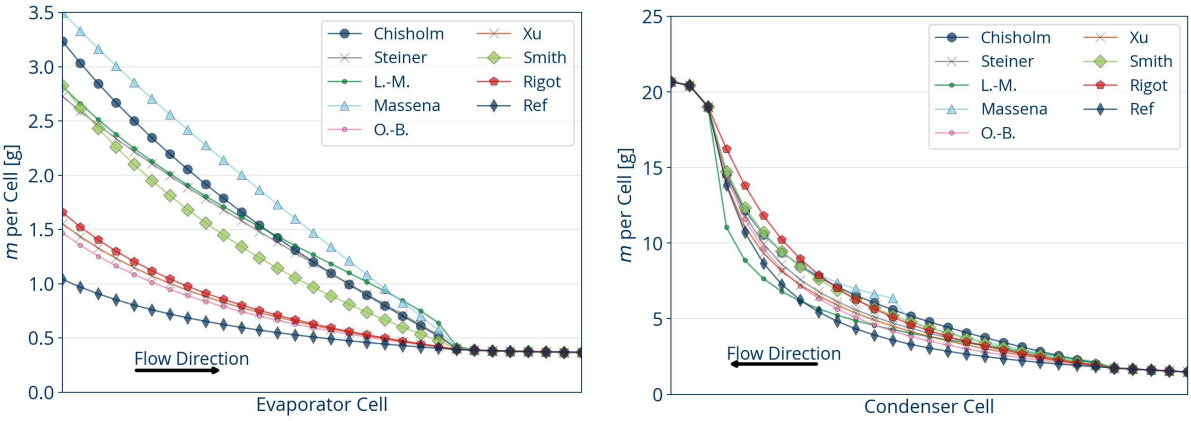

Figure 5: Mass distribution per cell in the evaporator (left) and condenser (right) at $\dot{Q}_H = 10$ kW

The reference case ($S = 1$) generally shows a lower mass than cases considering the velocity slip – except for the Lockhart-Martinelli model in the condenser. Moreover, the condenser tends to hold a higher refrigerant charge than the evaporator due to a lower average vapor quality (including subcooled liquid) and higher gas densities at a higher pressure level.

3.2 Analysis at Constant Refrigerant Charge

Another critical aspect is the influence of the velocity slip on overall system behavior when the refrigerant charge remains constant. In preparation for this investigation, the required refrigerant masses for the described R-290 heat pump for different heating capacity were determined in order to maintain 8 K subcooling based on the reference system (no slip). The determined charge was then fixed, and the slip ratio was adjusted using the eight chosen correlations.

Figure 6 (left) illustrates the influence of the different correlations on the cycle in the lg(p)-h diagram for $\dot{Q}_H = 10$ kW, while Figure 6 (right) shows the effect on subcooling for four different heating capacities. The presented "negative subcooling" represents the refrigerant being still within the two-phase region at the outlet of the condenser. This can be described with the following correlation:

$$SC = \frac{h_i - h(\dot{x} = 0)}{c_p(\dot{x} = 0)} \qquad \text{Eq. (18)}$$

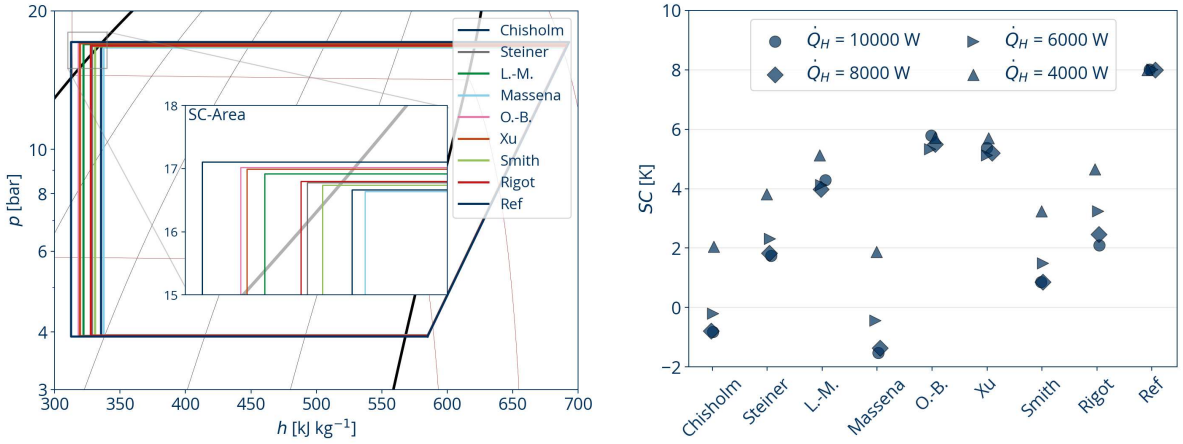

Figure 6: Influence of different slip correlations on the overall cycle for $\dot{Q}_H = 10$ kW (left) and subcooling for different heating capacities (right).

Depending on the slip model, varying degrees of subcooling are observed in the condenser. Since slip effects on heat transfer and pressure drop are not considered, the impact of slip ratios $S > 1$ on system pressures

and temperatures can be interpreted as a reduction in the effective refrigerant charge. An accumulation of refrigerant in the heat exchangers acts as if the system is undercharged, leading to reduced subcooling (see Figure 6, right) and a drop in system pressure (Figure 6, left).
For the models by Chisholm and Massena, this effect even leads to the complete disappearance of subcooling. The models from Xu and Osmachkin-Borisov exhibit the smallest variations, maintaining relatively stable subcooling across different heating capacities. This is because both correlations exhibit a higher slip ratio at lower heating capacities due to their dependence on the mass flow density (see Table 1). At the same time, the simulations show that at lower heating capacities, the influence of the velocity slip on subcooling becomes more pronounced. Applying the models according to Xu and Osmachkin-Borisov, these two effects nearly cancel each other out, resulting in minimal impact of heating capacity on subcooling.

3.3 Evaluation of the Influence of Different Refrigerants

In addition to the effect of the velocity slip on the overall cycle under different operating conditions, the influence within the heat exchanger for various refrigerants is also of interest, since some of the investigated slip correlations depend on the thermodynamic properties of the fluids. To study the refrigerant influence, the condenser of the previously described heat pump was simulated separately. The boundary conditions are listed in Table 3. The variables in this study were the refrigerant, the slip correlation, and the refrigerant mass flow rate.

Table 3: Boundary conditions for the investigation of refrigerant dependence of slip ratio

Condensation Temperature	50 °C
Inlet Superheat	5 K
Subcooling	0 K
Refrigerant Mass Flow	80 g/s, 20 g/s
Air Volume Flow	1 m^3/s
Refrigerants	R-717, R-600a, R-290, R-32, R-134a, R-410A
Air Temperature	Controlled to achieve 0 K subcooling

Figure 7 shows the mass-weighted average slip ratio $\bar{S}$ as a function of the refrigerant and the slip correlation at a refrigerant mass flow of 80 g/s.

Figure 7: Average slip ratio in the condenser as a function of slip correlation and refrigerant at $\dot{m} = 80$ g/s

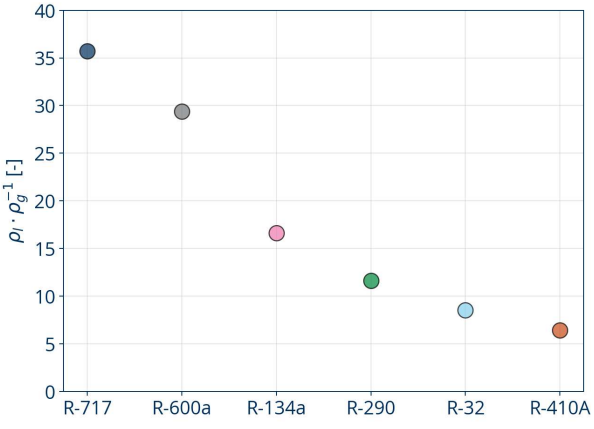

Figure 8: Density ratio of gas and liquid phase of the investigated refrigerants at 50 °C condensation temperature

Notably, there is a strong dependency of the velocity slip on the refrigerant – with the exception of the results of the correlations according Osmachkin-Borisov (O.-B.), Xu, and Rigot. The values for $\bar{S}$ are particularly low

for the refrigerants R-410A and R-32 (ranging between 1.1 and 2) and reach a maximum value of $\bar{S} = 4.2$ for R-717 with the correlation according to Massena. This distinct refrigerant sensitivity of $\bar{S}$ is primarily due to the different density ratios ρ_l / ρ_g of the refrigerants considered, which is illustrated in Figure 8 for the investigated condensation temperature.
Figure 9 further quantifies this behavior by showing the relative increase in the refrigerant charge $m_{rel.}$ in the heat exchanger compared to the homogeneous flow case of $\bar{S} = 1$.

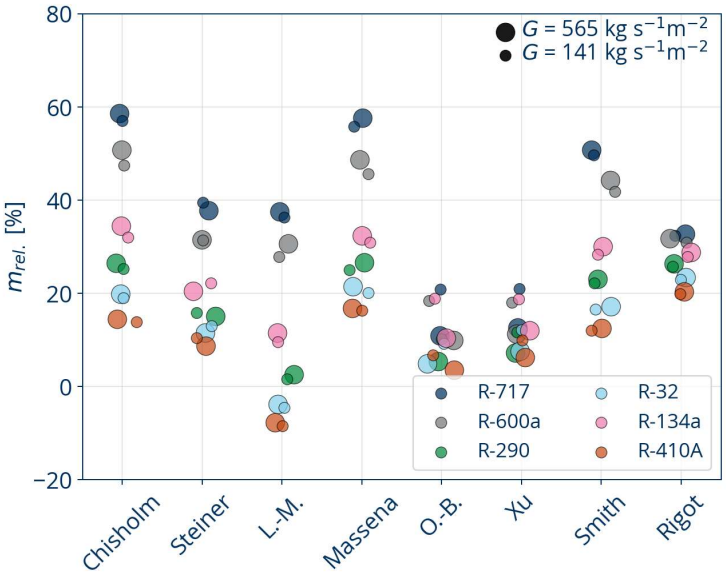

Figure 9: Relative increase in refrigerant charge in comparison to homogeneous flow as a function of refrigerant, slip correlation, and mass flux density G

Here, the variations with respect to the refrigerant are pronounced: R-410A, for example, shows only a modest increase (19 % with the Massena correlation), whereas R-717 exhibits the highest mass increase, reaching up to 59 %. The correlations that are less sensitive to refrigerant properties - namely by Osmachkin-Borisov, Xu, and Rigot - display minimal variations in the refrigerant charge. This is because, in those models, the slip ratio S is either constant (as in the correlation acc. to Rigot) or only minimally affected by the refrigerant properties. Yet even when S is held constant, the refrigerant charge still varies due to the refrigerant-specific liquid and gas densities (see Figure 8 and Eq. (19)). However, this density effect is relatively small compared to the overall impact of the slip ratio. Additionally, for correlations that do not depend on the mass flow, the influence of mass flow density on the relative charge increase is small and lacks a clear trend, as it primarily reflects differences in mass distribution from the heat transfer correlation acc. to Shah. In contrast, for the correlations acc. to Xu and Osmachkin-Borisov, higher mass fluxes yield a smaller slip ratio - that is, a larger void fraction vF - due to their dependency on the Froude number, which in turn reduces the extra relative refrigerant charge.

4 CONCLUSION AND OUTLOOK

In this study, the velocity slip in two-phase flows was successfully integrated into the balance equations of the TIL library for dynamic process simulations using the Modelica language. By simulating an air-to-air heat pump model under various operating conditions, the influence of the velocity slip could be analyzed in detail. Eight slip correlations were incorporated into the volume-discretized heat exchangers, allowing for the determination of local mass distributions and the required refrigerant charge at a constant subcooling. The results show that, compared to the reference case ($S = 1$), higher refrigerant charges are required when the velocity slip is considered – with an overall system mass increase between 5.7 % and 24.8 %, depending on the correlation. A volume-discrete analysis of the slip-dependent mass distribution in both the condenser

and evaporator revealed clear differences compared to calculations neglecting the velocity slip. Furthermore, it was demonstrated that considering the velocity slip influences the behavior of subcooling: depending on the correlation used, subcooling was significantly reduced or even completely eliminated compared to the 8 K observed in the reference case.

In addition, the influence of the correlations on the mass distribution in the condenser for different refrigerants was investigated. The correlations by Massena, Lockhart-Martinelli, and Chisholm showed a strong dependence of the mass increase on the refrigerant, which can be attributed to the differing density ratios between liquid and gas. In contrast, the correlations by Xu and Osmachkin-Borisov proved to be comparatively insensitive to refrigerant variations.

Future work should also investigate the transient effects of the velocity slip, particularly with regard to the control behavior of compressors and expansion valves. Additionally, it would also be worth investigating how the velocity slip influences pressure loss and heat transfer by taking into account the difference between circulating and local fluid properties. These investigations could lead to a better prediction and adaptation of the operating strategy and thus further increase the efficiency and reliability of refrigeration systems and heat pumps.

ACKNOWLEDGEMENTS

The authors express their gratitude to Mr. Manuel Gräber from TLK Energy, whose expertise and thoughtful discussions enriched this research.

NOMENCLATURE

List of Symbols		SH	Superheat (K)
C_0	Distribution Parameter (-)	t	Time (s)
D	Diameter (m)	T / t	Absolute/Relative Temperature (K/°C)
Fr	Froude Number (-)	w	Velocity ($m \cdot s^{-1}$)
g	Gravitational Acceleration ($m \cdot s^{-2}$)	V	Volume (m^3)
G	Mass Flux ($kg \cdot m^{-2} \cdot s^{-1}$)	vF	Void Fraction (–)
h	Specific Enthalpy ($J \cdot kg^{-1}$)	x	Local Vapor Mass Fraction (-)
K	Correction Factor (-)	X_{tt}	Lockhart-Martinelli Parameter (-)
m	Mass (kg)	η	Dynamic Viscosity (Pa·s)
n	Rotational Speed (s^{-1})	ρ	Density ($kg \cdot m^{-3}$)
p	Pressure (Pa)	$\bar{S}$	Average Slip Ratio (-)
P_i	Indicated Power (W)	$\dot{Q}$	Power (thermal) (W)
S	Slip Ratio (-)	$\dot{m}$	Mass Flow ($kg \cdot s^{-1}$)
SC	Subcooling (K)	$\dot{x}$	Vapor Mass Fraction in the flow
σ	Surface Tension ($J \cdot m^{-1}$)	c_p	Specific Isobaric Heat Capacity
COP	Coefficient of Performance (-)		

Indices		H	Heating
0	Evaporation State	h	Homogeneous
A	Inlet State	i	Index Variable
B	Outlet State	l	Liquid
c	Condensation State	m	Mean
cr	Critical	ref	Reference
g	Gaseous	rel.	Relative
tot	Total	sg	Superficial (gas)
gm	Drift		

REFERENCES

TLK Thermo GmbH, 2024, *TIL Suite - Thermodynamik Simulation*. Modelica. TLK Energy, Aachen. [Online]. Available at: https://tlk-energy.de/software/til-suite

G. L. Wedekind, B. L. Bhatt, and B. T. Beck, 1978, „A system mean void fraction model for predicting various transient phenomena associated with two-phase evaporating and condensing flows“, *International Journal of Multiphase Flow*, Bd. 4, Nr. 1, S. 97–114, doi: 10.1016/0301-9322(78)90029-0.

R. Shah, A. G. Alleyne, and C. W. Bullard, 2004, „Dynamic Modeling and Control of Multi-Evaporator Air-Conditioning Systems“, *ASHRAE Transactions*.

B. P. Rasmussen,2012, „Dynamic modeling for vapor compression systems—Part I: Literature review“, *HVAC&R Research*, Bd. 18, Nr. 5, S. 934–955, doi: 10.1080/10789669.2011.582916.

K. Assawamartbunlue und M. J. Brandemuehl, 2000, „The Effect of Void Fraction Models and Heat Flux Assumption on Predicting Refrigerant Charge Level in Receivers“, International Refrigeration and Air Conditioning Conference. Paper 519.

O. Abdelaziz, V. Aute, and R. Radermacher, 2008, „Effect of Void Fraction Model on the Dynamic Performance of Moving Boundary Heat Exchanger“, International Refrigeration and Air Conditioning Conference. Paper 991

VDI e. V., Hrsg., *VDI-Wärmeatlas*. Berlin, Heidelberg: Springer Berlin Heidelberg, 2013. doi: 10.1007/978-3-642-19981-3.

D. M. Graham und J. C. Chato, 1997, „Experimental Investigation of Void Fraction During Refrigerant Condensation“, Air Conditioning and Refrigeration Center TR-135

M. J. Wilson, T. A. Newell, and J. C. Chato, 1998, „Experimental Investigation of Void Fraction During Horizontal Flow in Larger Diameter Refrigeration Applications“, Air Conditioning and Refrigeration Center TR-140

C. K. Rice, 1987, „The effect of void fraction correlation and heat flux assumption on refrigerant charge inventory predictions“, *Ashrae Transactions*, accessed October 31, 2024. [Online]. Available at: https://www.semanticscholar.org/paper/The-effect-of-void-fraction-correlation-and-heat-on-Rice/325b088efcdb9d6b3e7fa865e02df826bc804021

Y. Xu and X. Fang, 2014, „Correlations of void fraction for two-phase refrigerant flow in pipes“, *Applied Thermal Engineering*, Bd. 64, Nr. 1–2, S. 242–251, doi: 10.1016/j.applthermaleng.2013.12.032.

D. Chisholm, 1973, „Research Note: Void Fraction During Two-Phase Flow“, Available at: https://journals.sagepub.com/doi/abs/10.1243/JMES_JOUR_1973_015_040_02?journalCode=jmsa

S. L. Smith, 1969, „Void Fractions in Two-Phase Flow: A Correlation Based upon an Equal Velocity Head Model“, *Proceedings of the Institution of Mechanical Engineers*, Bd. 184, Nr. 1, S. 647–664, doi: 10.1243/PIME_PROC_1969_184_051_02.

B. Shen, J. E. Braun, and E. A. Groll, 2009, „Improved methodologies for simulating unitary air conditioners at off-design conditions“, *International Journal of Refrigeration*, Bd. 32, Nr. 7, S. 1837–1849, doi: 10.1016/j.ijrefrig.2009.06.009.

M. M. Shah, 1979, „A general correlation for heat transfer during film condensation inside pipes“, *International Journal of Heat and Mass Transfer*, Bd. 22, Nr. 4, S. 547–556, doi: 10.1016/0017-9310(79)90058-9.

H. D. Baehr and K. Stephan, 1996, *Wärme- und Stoffübertragung*, 2. Auflage

F. Steimle and K. Stephan, 1988, *Handbuch der Kältetechnik. Bd. 6, Teil B: Wärmeaustauscher / hrsg. von Fritz Steimle und K. Stephan*, Softcover reprint of the hardcover 1st edition 1988., Bd. 6. Berlin: Springer, 1988.

APPENDIX

Table 4: Volumes of the heat pump

Section	Volume (l)	Relative to Total Volume (%)
Discharge Gas Line + High-Pressure Compressor Volume	0.534	9
Condenser	1.35	22
Liquid Line	0.025	< 1
Evaporator Inlet	0.016	< 1
Evaporator	1.35	22
Compressor + Suction Gas Line	2.82	46
Total	6.1	100